

# 17. FRAGMENTATION FUNCTIONS IN $e^+e^-$ , $ep$ AND $pp$ COLLISIONS

Revised October 2009 by O. Biebel (Ludwig-Maximilians-Universität, Munich, Germany), D. de Florian (Dep. de Física, FCEyN-UBA, Buenos Aires, Argentina), D. Milstead (Fysikum, Stockholms Universitet, Sweden), and A. Vogt (Dep. of Mathematical Sciences, University of Liverpool, UK).

## 17.1. Introduction to fragmentation

The term ‘fragmentation functions’ is widely used for two related if conceptually different sets of functions describing final-state single particle energy distributions in hard scattering processes (see Refs. [1,2] for introductory reviews, and Refs. [3,4] for summaries of recent experimental and theoretical research in this field).

The first are cross-section observables such as the functions  $F_{T,L,A}(x, s)$  in semi-inclusive  $e^+e^-$  annihilation at center-of-mass (CM) energy  $\sqrt{s}$  via an intermediate photon or  $Z$ -boson,  $e^+e^- \rightarrow \gamma/Z \rightarrow h + X$ , given by

$$\frac{1}{\sigma_0} \frac{d^2\sigma^h}{dx d\cos\theta} = \frac{3}{8}(1 + \cos^2\theta)F_T^h + \frac{3}{4}\sin^2\theta F_L^h + \frac{3}{4}\cos\theta F_A^h. \quad (17.1)$$

Here  $x = 2E_h/\sqrt{s} \leq 1$  is the scaled energy of the hadron  $h$  (in practice the approximation  $x \simeq x_p = 2p_h/\sqrt{s}$  is often used), and  $\theta$  is its angle relative to the electron beam in the CM frame. Eq. (17.1) is the most general form for unpolarized inclusive single-particle production via vector bosons [5]. The transverse and longitudinal fragmentation functions  $F_T$  and  $F_L$  represent the contributions from  $\gamma/Z$  polarizations transverse or longitudinal with respect to the direction of motion of the hadron. The parity-violating term with the asymmetric fragmentation function  $F_A$  arises from the interference between vector and axial-vector contributions. Normalization factors  $\sigma_0$  used in the literature range from the total cross section  $\sigma_{\text{tot}}$  for  $e^+e^- \rightarrow$  hadrons, including all weak and QCD contributions, to  $\sigma_0 = 4\pi\alpha^2 N_c/3s$  with  $N_c = 3$ , the lowest-order QED cross section for  $e^+e^- \rightarrow \mu^+\mu^-$  times the number of colors  $N_c$ . LEP1 measurements of all three fragmentation functions are shown in Fig. 17.1.

## 2 17. Fragmentation functions in $e^+e^-$ , $ep$ and $pp$ collisions

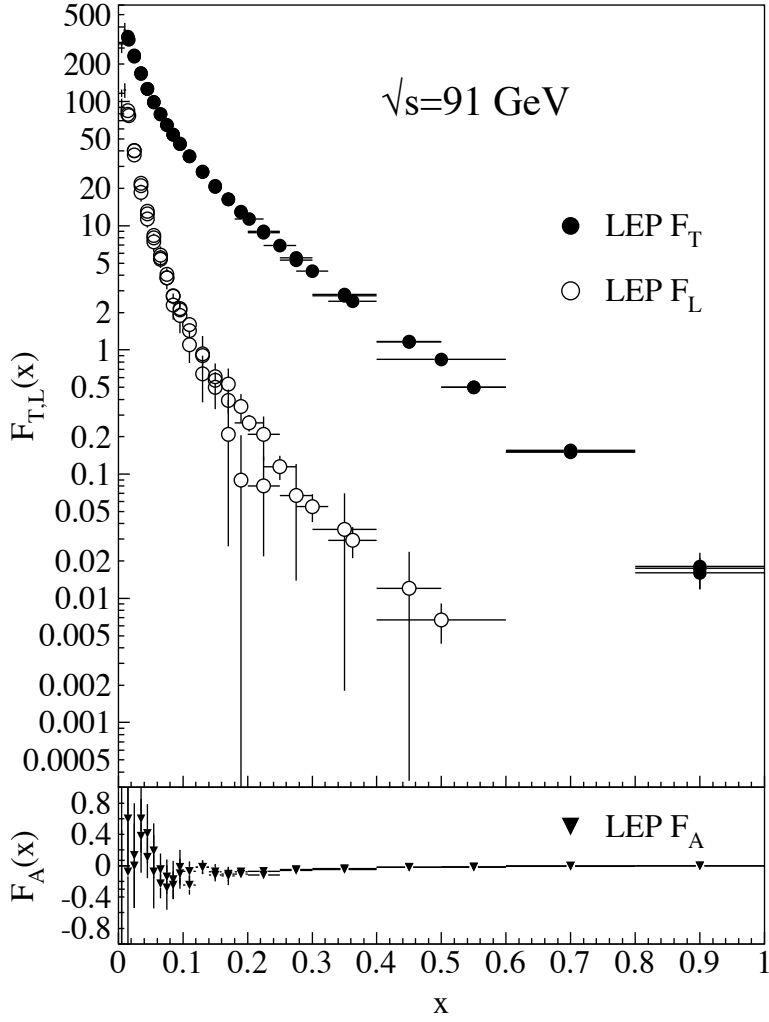


**Figure 17.1:** LEP1 measurements of total transverse ( $F_T$ ), longitudinal ( $F_L$ ), and asymmetric ( $F_A$ ) fragmentation functions [6,7,8]. Data points with relative errors greater than 100% are omitted.

Integration of Eq. (17.1) over  $\theta$  yields the total fragmentation function  $F^h = F_T^h + F_L^h$ ,

$$\frac{1}{\sigma_0} \frac{d\sigma^h}{dx} = F^h(x, s) = \sum_i \int_x^1 \frac{dz}{z} C_i(z, \alpha_s(\mu), \frac{s}{\mu^2}) D_i^h(\frac{x}{z}, \mu^2) + \mathcal{O}(\frac{1}{\sqrt{s}}) \quad (17.2)$$

with  $i = u, \bar{u}, d, \bar{d}, \dots, g$ . Here we have introduced the second set of functions mentioned in the first paragraph, the parton fragmentation functions (or fragmentation densities)  $D_i^h$ . These functions are the final-state analogue of the initial-state parton distributions addressed in Section 16 of this *Review*. Due to the different sign of the squared four-momentum  $q^2$  of the intermediate gauge boson these two sets of distributions are also referred to as the timelike ( $e^+e^-$  annihilation,  $q^2 > 0$ ) and spacelike (deep-inelastic scattering (DIS),  $q^2 < 0$ ) parton distributions. The function  $D_i^h(z, \mu^2)$  encodes the probability that the parton  $i$  fragments into a hadron  $h$  carrying a fraction  $z$  of the parton's momentum. Beyond the leading order (LO) of perturbative QCD these universal

functions are factorization-scheme dependent, with ‘reasonable’ scheme choices retaining certain quark-parton-model (QPM) constraints such as the momentum sum rule

$$\sum_h \int_0^1 dz z D_i^h(z, \mu^2) = 1. \quad (17.3)$$

The dependence of the functions  $D_i^h$  on the factorization (or fragmentation) scale  $\mu^2$  (in Eq. (17.2) and below identified with the renormalization scale) is discussed in Section 17.2.

The second ingredient in Eq. (17.2), and analogous expressions for the functions  $F_{T,L,A}$ , are the observable-dependent coefficient functions  $C_i$ . At the zeroth order in the strong coupling  $\alpha_s$  the coefficient functions  $C_g$  for gluons are zero, while for (anti-) quarks  $C_i = g_i(s) \delta(1 - z)$  except for  $F_L$ , where  $g_i(s)$  is the appropriate electroweak coupling. In particular,  $g_i(s)$  is proportional to the squared charge of the quark  $i$  at  $s \ll M_Z^2$ , when weak effects can be neglected. The full electroweak prefactors  $g_i(s)$  can be found in Ref. [5]. The power corrections in Eq. (17.2) arise from quark and hadron mass terms and from non-perturbative effects.

Measurements of fragmentation in lepton-hadron and hadron-hadron scattering are complementary to those in  $e^+e^-$  annihilation. The latter provides a clean environment (no initial-state hadron remnant) and stringent constraints on the combinations  $D_{q_i}^h + D_{\bar{q}_i}^h$ . However  $e^+e^-$  annihilation is far less sensitive to  $D_g^h$  and insensitive to the charge asymmetries  $D_{q_i}^h - D_{\bar{q}_i}^h$ . These quantities are best constrained in proton-(anti-)proton and electron-proton scattering, respectively. Especially the latter provides a more complicated environment with which it is possible to study the influence on the fragmentation process from initial state QCD radiation, the partonic and spin structure of the hadron target, and the target remnant system (see Ref. [9] for a comprehensive review of the measurements and models of fragmentation in lepton-hadron scattering).

Moreover, unlike  $e^+e^-$  annihilation where  $q^2 = s$  is fixed by the collider energy, lepton-hadron scattering has two independent scales,  $Q^2 = -q^2$  and the invariant mass  $W^2$  of the hadronic final state, which both can vary by several orders of magnitudes for a given CM energy, thus allowing the study of fragmentation in different environments by a single experiment. E.g., in photoproduction the exchanged photon is quasi-real ( $Q^2 \approx 0$ ) leading to processes akin to hadron-hadron scattering. In DIS ( $Q^2 \gg 1 \text{ GeV}^2$ ), using the QPM, the hadronic fragments of the struck quark can be directly compared with quark fragmentation in  $e^+e^-$  in a suitable frame. Results from lepton-hadron experiments quoted in this report primarily concern fragmentation in the DIS regime. Studies performed by lepton-hadron experiments of fragmentation with photoproduction data containing high transverse momentum jets or particles are also reported, when these are directly comparable to DIS and  $e^+e^-$  results.

Fragmentation studies at HERA are usually performed in one of two frames in which the target hadron and the exchanged boson are collinear. The hadronic center-of-mass frame (HCMS) is defined as the rest system of the exchanged boson and incoming hadron, with the  $z^*$ -axis defined along the direction of the exchanged boson. The positive  $z^*$

## 4 17. Fragmentation functions in $e^+e^-$ , $ep$ and $pp$ collisions

direction defines the so-called current region. Fragmentation measurements performed in the HCMS often use the Feynman- $x$  variable  $x_F = 2p_z^*/W$ , where  $p_z^*$  is the longitudinal momentum of the particle in this frame. As  $W$  is the invariant mass of the hadronic final state,  $x_F$  ranges between  $-1$  and  $1$ .

The Breit system [10] is connected to the HCMS by a longitudinal boost such that the time component of  $q$  vanishes, i.e.,  $q = (0, 0, 0, -Q)$ . In the QPM, the struck parton then has the longitudinal momentum  $Q/2$  which becomes  $-Q/2$  after the collision. As compared with the HCMS, the current region of the Breit frame is more closely matched to the partonic scattering process, and is thus appropriate for direct comparisons of fragmentation functions in DIS with those from  $e^+e^-$  annihilation. The variable  $x_p = 2p^*/Q$  is used at HERA for measurements in the Breit frame, ensuring rather directly comparable DIS and  $e^+e^-$  results, where  $p^*$  is the particle's momentum in the current region of the Breit frame.

### 17.2. Scaling violation

The simplest parton-model approach would predict scale-independent  $x$ -distributions ('scaling') for both the fragmentation function  $F^h$  and the parton fragmentation functions  $D_i^h$ . Perturbative QCD corrections lead, after factorization of the final-state collinear singularities for light partons, to logarithmic scaling violations via the evolution equations

$$\frac{\partial}{\partial \ln \mu^2} D_i(x, \mu^2) = \sum_j \int_x^1 \frac{dz}{z} P_{ji}(z, \alpha_s(\mu^2)) D_j\left(\frac{x}{z}, \mu^2\right). \quad (17.4)$$

Usually this system of equations is decomposed into a  $2 \times 2$  flavour-singlet sector comprising gluon and the sum of all quark and antiquark fragmentation functions, and scalar ('non-singlet') equations for quark-antiquark and flavour differences. Notice that the singlet splitting-function matrix is now  $P_{ji}$ , rather than  $P_{ij}$  as for the initial-state parton distributions, since  $D_j$  represents the fragmentation of the final parton.

The splitting functions in Eq. (17.4) have perturbative expansion of the form

$$P_{ji}(z, \alpha_s) = \frac{\alpha_s}{2\pi} P_{ji}^{(0)}(z) + \left(\frac{\alpha_s}{2\pi}\right)^2 P_{ji}^{(1)}(z) + \left(\frac{\alpha_s}{2\pi}\right)^3 P_{ji}^{(2)}(z) + \dots \quad (17.5)$$

where the leading-order (LO) functions  $P^{(0)}(z)$  [11,12] are the same as those for the initial-state parton distributions. The next-to-leading order (NLO) corrections  $P^{(1)}(z)$  have been calculated in Refs. [13–17] (there are well-known misprints in the journal version of Ref. [14]). Ref. [17] also includes the spin-dependent case. These functions are different from, but related to their space-like counterparts, see also Ref. [18]. These relations have facilitated recent calculations of the next-to-next-to-leading order (NNLO) quantities  $P_{qq}^{(2)}(z)$  and  $P_{gg}^{(2)}(z)$  in Eq. (17.5) [19,20]. The corresponding off-diagonal quantities  $P_{qg}^{(2)}$  and  $P_{gq}^{(2)}$  are not yet known except for their second moments fixed by the momentum sum rule, Eq. (17.3) [20]. All these results refer to the standard  $\overline{\text{MS}}$  scheme,

with the exception of Refs. [16], with a fixed number  $n_f$  of light flavours. The NLO treatment of flavour thresholds in the evolution has been addressed in Ref. [21].

The QCD parts of the coefficient functions for  $F_{T,L,A}(x,s)$  in Eq. (17.1) and the total fragmentation function  $F_2^h \equiv F^h$  in Eq. (17.2) are given by

$$C_{a,i}(z, \alpha_s) = (1 - \delta_{aL}) \delta_{iq} + \frac{\alpha_s}{2\pi} c_{a,i}^{(1)}(z) + \left(\frac{\alpha_s}{2\pi}\right)^2 c_{a,i}^{(2)}(z) + \dots . \quad (17.6)$$

The first-order corrections have been calculated a long time ago in Refs. [22], and the second-order terms in [23]. The latter results have recently been verified (and some typos corrected) in Refs. [19,24]. Thus the coefficient functions are known to NNLO except for  $F_L$  where the leading contribution is of order  $\alpha_s$ .

The effect of the evolution is similar in the timelike and spacelike cases: as the scale increases, one observes a scaling violation in which the  $x$ -distribution is shifted towards lower values. This can be seen from Fig. 17.2 where a large amount of measurements of the total fragmentation function in  $e^+e^-$  annihilation are summarized. QCD analyses of these data are discussed in Section 17.5 below.

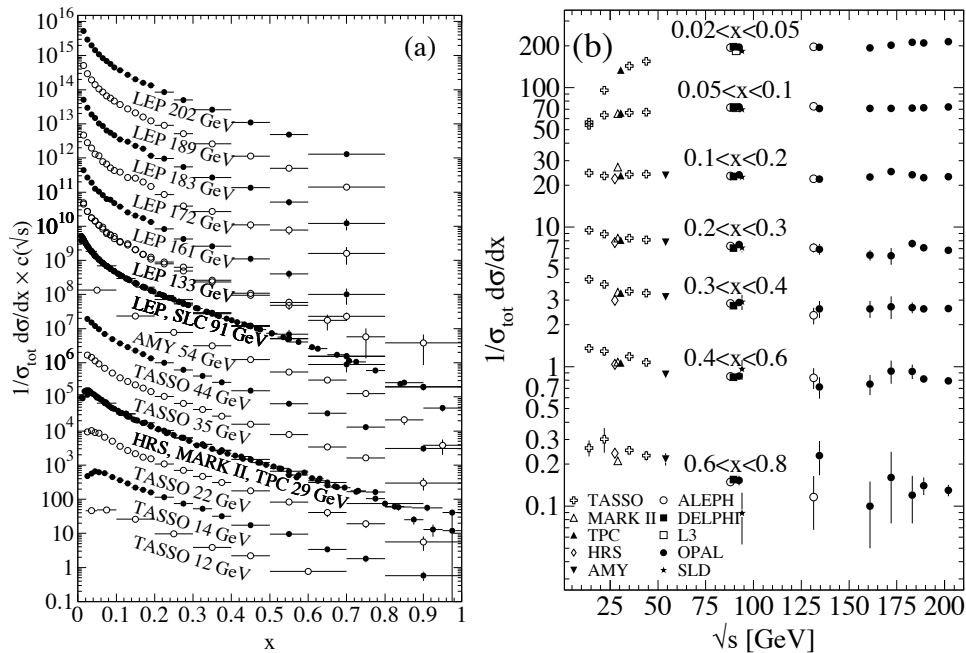


**Figure 17.2:** The  $e^+e^-$  fragmentation function for all charged particles is shown [8,25–41] (a) for different CM energies  $\sqrt{s}$  versus  $x$  and (b) for various ranges of  $x$  versus  $\sqrt{s}$ . For the purpose of plotting (a), the distributions were scaled by  $c(\sqrt{s}) = 10^i$  with  $i$  ranging from 0 ( $\sqrt{s} = 12$  GeV) to 13 ( $\sqrt{s} = 202$  GeV).

Unlike the splitting functions in Eq. (17.5), see Refs. [18–20], the coefficient functions for  $F_{2,T,A}$  in Eq. (17.6) show a threshold enhancement with terms up to

## 6 17. Fragmentation functions in $e^+e^-$ , $ep$ and $pp$ collisions

$\alpha_s^n(1-z)^{-1} \ln^{2n-1}(1-z)$ . Such logarithms can be resummed to all orders in  $\alpha_s$  using standard soft-gluon techniques [42–44]. Recently this resummation has been extended to the subleading (and for  $F_L$  leading) class  $\alpha_s^n \ln^k(1-z)$  of large- $x$  logarithms [45].

In Refs. [22] the NLO coefficient functions have been calculated also for single hadron production in lepton-proton scattering,  $ep \rightarrow e + h + X$ . More recently corresponding results have been obtained for the case that a non-vanishing transverse momentum is required in the HCMS frame [46].

Scaling violations in DIS are shown in Fig. 17.3 for both HCMS and Breit frame. In Fig. 1.3(a) the distribution in terms of  $x_F = 2p_z^*/W$  shows a steeper slope in  $ep$  data than for the lower-energy  $\mu p$  data for  $x_F > 0.15$ , indicating the scaling violations. At smaller values of  $x_F$  in the current jet region, the multiplicity of particles substantially increases with  $W$  owing to the increased phase space available for the fragmentation process. The EMC data access both the current region and the region of the fragmenting target remnant system. At higher values of  $|x_F|$ , due to the extended nature of the remnant, the multiplicity in the target region far exceeds that in the current region. For acceptance reasons the remnant hemisphere of the HCMS is only accessible by the lower-energy fixed-target experiments.

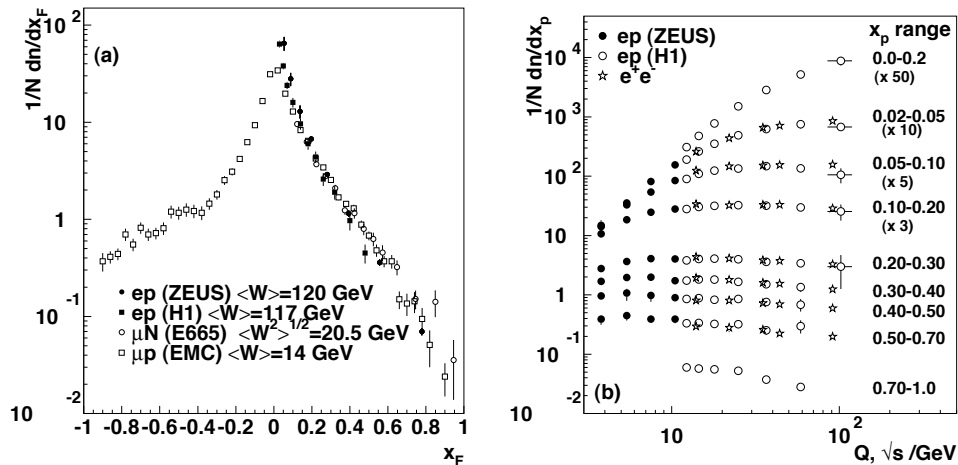


**Figure 17.3:** (a) The distribution  $1/N \cdot dN/dx_F$  for all charged particles in DIS lepton-hadron experiments at different values of  $W$ , and measured in the HCMS [47–50]. (b) Scaling violations of the fragmentation function for all charged particles in the current region of the Breit frame of DIS [51,56] and in  $e^+e^-$  interactions [40,57]. The data are shown as a function of  $\sqrt{s}$  for  $e^+e^-$  results, and as a function of  $Q$  for the DIS results, each within the same indicated intervals of the scaled momentum  $x_p$ . The data for the four lowest intervals of  $x_p$  are multiplied by factors 50, 10, 5, and 3, respectively for clarity.

Using hadrons from the current hemisphere in the Breit frame, measurements of fragmentation functions and the production properties of particles in  $ep$  scattering have been made by Refs. [51–56]. Fig. 17.3(b) compares results from  $ep$  scattering and  $e^+e^-$  experiments, the latter results are halved as they cover both event hemispheres. The

agreement between the DIS and  $e^+e^-$  results is fairly good. However, processes in DIS which are not present in  $e^+e^-$  annihilation, such as boson-gluon fusion and initial state QCD radiation, can depopulate the current region. These effects become most prominent at low values of  $Q$  and  $x_p$ . Hence, when compared with  $e^+e^-$  annihilation data at  $\sqrt{s} = 5.2, 6.5$  GeV [58] not shown here, the DIS particle rates tend to lie below those from  $e^+e^-$  annihilation. A recent ZEUS study [59] finds that the direct comparability of the  $ep$  data to  $e^+e^-$  results at low scales is improved if twice the energy in the current hemisphere of the Breit frame,  $2E_B^{\text{cr}}$ , is used instead of  $Q$  as the fragmentation scale.

### 17.3. Fragmentation functions for small particle momenta

The higher-order timelike splitting functions in Eq. (17.5) are very singular at small  $x$ . They show a double-logarithmic (LL) enhancement with leading terms of the form  $\alpha_s^n \ln^{2n-2} x$  corresponding to poles  $\alpha_s^n (N-1)^{1-2n}$  for the Mellin moments

$$P^{(n)}(N) = \int_0^1 dx x^{N-1} P^{(n)}(x). \quad (17.7)$$

Despite large cancellations between leading and non-leading logarithms at non-asymptotic value of  $x$ , the resulting small- $x$  rise in the timelike splitting functions dwarfs that of their spacelike counterparts for the evolution of the parton distributions in Section 16 of this *Review*, see Fig. 1 of Ref. [20]. Consequently the fixed-order approximation to the evolution breaks down orders of magnitude in  $x$  earlier in fragmentation than in DIS.

The pattern of the known coefficients and other considerations suggest that the LL terms sum to all-order expressions without any pole at  $N = 1$  such as [60,61]

$$P_{gg}^{\text{LL}}(N) = -\frac{1}{4}(N-1 - \sqrt{(N-1)^2 \cdot 24 \alpha_s/\pi}). \quad (17.8)$$

Keeping the first three terms in the resulting expansion of Eq. (17.4) around  $N = 1$  yields a Gaussian in the variable  $\xi = \ln(1/x)$  for the small- $x$  fragmentation functions,

$$xD(x, s) \propto \exp \left[ -\frac{1}{2\sigma^2} (\xi - \xi_p)^2 \right], \quad (17.9)$$

with the peak position and width varying with the energy as [62] (see also Ref. [2])

$$\xi_p \simeq \frac{1}{4} \ln \left( \frac{s}{\Lambda^2} \right), \quad \sigma \propto \left[ \ln \left( \frac{s}{\Lambda^2} \right) \right]^{3/4}. \quad (17.10)$$

Next-to-leading corrections to the above predictions have been calculated [63]. In the method of Ref. [64], see also Refs. [65,66], the corrections are included in an analytical form known as the ‘modified leading logarithmic approximation’ (MLLA). Alternatively they can be used to compute higher-moment corrections to the shape in Eq. (17.9) [67].

Fig. 17.4 shows the  $\xi$  distribution for charged particles produced in the current region of the Breit frame in DIS and in  $e^+e^-$  annihilation. Consistent with Eq. (17.9) (the ‘hump backed plateau’) and Eq. (17.10) the distributions have a Gaussian shape with the peak position and area increasing with the CM energy ( $e^+e^-$ ) and  $Q^2$  (DIS).

## 8 17. Fragmentation functions in $e^+e^-$ , $ep$ and $pp$ collisions

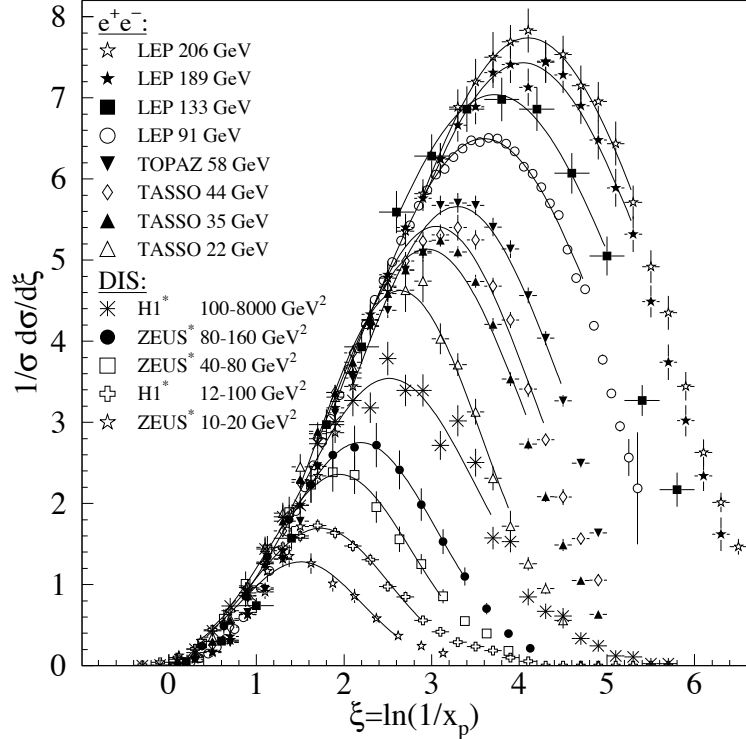


**Figure 17.4:** Distribution of  $\xi = \ln(1/x_p)$  at several CM energies ( $e^+e^-$ ) [25–27,32–35,40,68–71] and intervals of  $Q^2$  (DIS) [54,55]. At each energy only one representative measurement is displayed. For clarity some measurements at intermediate CM energies ( $e^+e^-$ ) or  $Q^2$  ranges (DIS) are not shown. The DIS measurements (\*) have been scaled by a factor of 2 for direct comparability with the  $e^+e^-$  results. Fits of simple Gaussian functions are overlaid for illustration.

The predicted energy dependence Eq. (17.10) of the peak in the  $\xi$  distribution is explained by soft gluon coherence (angular ordering) which correctly predicts the suppression of hadron production at small  $x$ . Of course, a decrease at very small  $x$  is expected on purely kinematical grounds, but this would occur at particle energies proportional to their masses, *i.e.*, at  $x \propto m/\sqrt{s}$  and hence  $\xi \sim \frac{1}{2} \ln s$ . Thus, if the suppression were purely kinematic, the peak position  $\xi_p$  would vary twice as rapidly with the energy, which is ruled out by the data in Fig. 17.5. The  $e^+e^-$  and DIS data agree well with each other, demonstrating the universality of hadronization, and the MLLA prediction. Measurements of the higher moments of the  $\xi$  distribution in  $e^+e^-$  [40,71–73] and DIS [55] have also been performed and show consistency with each other.

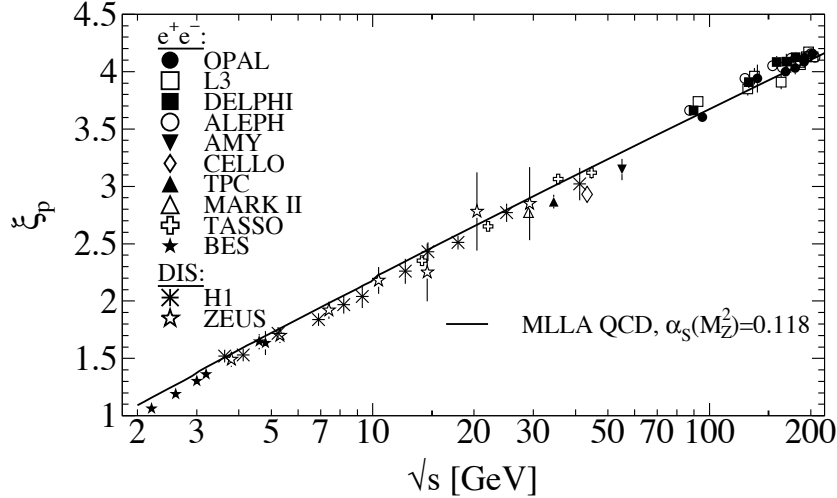


**Figure 17.5:** Evolution of the peak position,  $\xi_p$ , of the  $\xi$  distribution with the CM energy  $\sqrt{s}$ . The MLLA QCD prediction using  $\alpha_S(s = M_Z^2) = 0.118$  is superimposed to the data of Refs. [25,27,28,31–33,35,40,53,54,69,70,73–81].

## 17.4. Fragmentation models

Although the scaling violation can be calculated perturbatively, the actual form of the parton fragmentation functions is non-perturbative. Perturbative evolution gives rise to a shower of quarks and gluons (partons). Multi-parton final states from leading and higher order matrix element calculations are linked to these parton showers using factorization prescriptions, also called matching schemes, see Ref. [82] for an overview. Phenomenological schemes are then used to model the carry-over of parton momenta and flavor to the hadrons. Two of the very popular models are the *string fragmentation* [83,84], implemented in the JETSET [85], PYTHIA [86] and UCLA [87] Monte Carlo event generation programs, and the *cluster fragmentation* of the HERWIG [88] and SHERPA [89] Monte Carlo event generators.

**17.4.1. String fragmentation :** The string-fragmentation scheme considers the color field between the partons, *i.e.*, quarks and gluons, to be the fragmenting entity rather than the partons themselves. The string can be viewed as a color flux tube formed by gluon self-interaction as two colored partons move apart. Energetic gluon emission is regarded as energy-momentum carrying “kinks” on the string. When the energy stored in the string is sufficient, a  $q\bar{q}$  pair may be created from the vacuum. Thus, the string breaks up repeatedly into color singlet systems, as long as the invariant mass of the string pieces exceeds the on-shell mass of a hadron. The  $q\bar{q}$  pairs are created according to the probability of a tunneling process  $\exp(-\pi m_{q,\perp}^2/\kappa)$ , which depends on the transverse mass squared  $m_{q,\perp}^2 \equiv m_q^2 + p_{q,\perp}^2$  and the string tension  $\kappa \approx 1$  GeV/fm. The transverse momentum  $p_{q,\perp}$  is locally compensated between quark and antiquark. Due to the dependence on the parton mass,  $m_q$ , and/or hadron mass,  $m_h$ , the production of strange and, in particular, heavy-quark hadrons is suppressed. The light-cone momentum fraction  $z = (E + p_{\parallel})_h/(E + p)_q$ , where  $p_{\parallel}$  is the momentum of the formed hadron  $h$  along the

## 10 17. Fragmentation functions in $e^+e^-$ , $ep$ and $pp$ collisions

direction of the quark  $q$ , is given by the string-fragmentation function

$$f(z) \sim \frac{1}{z} (1-z)^a \exp\left(-\frac{bm_{h,\perp}^2}{z}\right), \quad (17.11)$$

where  $a$  and  $b$  are free parameters. These parameters need to be adjusted to bring the fragmentation into accordance with measured data, *e.g.*,  $a = 0.11$  and  $b = 0.52 \text{ GeV}^{-2}$  as determined in [90] (for an overview on tuned parameters see [91]).

**17.4.2. Cluster fragmentation :** Assuming a local compensation of color based on the *pre-confinement* property of perturbative QCD [92], the remaining gluons at the end of the parton shower evolution are split non-perturbatively into quark-antiquark pairs. Color singlet clusters of typical mass of a couple of GeV are then formed from quark and antiquark of color-connected splittings. These clusters decay directly into two hadrons unless they are either too heavy, when they decay into two clusters, or too light, in which case a cluster decays into a single hadron, requiring a small rearrangement of energy and momentum with neighboring clusters. The decay of a cluster into two hadrons is assumed to be isotropic in the rest frame of the cluster except if a perturbative-formed quark is involved. A decay channel is chosen based on the phase-space probability, the density of states, and the spin degeneracy of the hadrons. Cluster fragmentation has a compact description with few parameters, due to the phase-space dominance in the hadron formation.

## 17.5. Quark and gluon fragmentation functions

The fragmentation functions are solutions to the evolution equations Eq. (17.4), but need to be parametrized at some initial scale  $\mu_0^2$  (usually around  $1 \text{ GeV}^2$  for light quarks and gluons and  $m_Q^2$  for heavy quarks). A usual parametrization for light hadrons is [93–98]

$$D_i^h(x, \mu_0^2) = Nx^\alpha(1-x)^\beta \left(1 + \gamma(1-x)^\delta\right), \quad (17.12)$$

where the normalization  $N$ , and the parameters  $\alpha$ ,  $\beta$ ,  $\gamma$  and  $\delta$  in general depend on the energy scale  $\mu_0^2$ , and also on the type of the parton,  $i$ , and the hadron,  $h$ . Frequently the term involving  $\gamma$  and  $\delta$  is left out [95–98]. Heavy flavor fragmentation into heavy mesons is discussed in Sect. 17.9. The parameters of Eq. (17.12) (see [93–98]) are obtained by performing global fits to data on various hadron types for different combinations of partons and hadrons in  $e^+e^-$ , lepton-hadron and hadron-hadron collisions.

Data from  $e^+e^-$  annihilation present the cleanest experimental source for the measurement of fragmentation functions, but can not contribute to disentangle quark from antiquark distributions. Since the bulk of the  $e^+e^-$  annihilation data is obtained at the mass of the  $Z$ -boson, where the electroweak couplings are roughly the same for the different partons, it provides the most precise determination of the flavor-singlet quark fragmentation. Flavor tagged results [99], distinguishing between the light quark, charm and bottom contributions are of particular value for flavor decomposition, even though those measurements can not be unambiguously interpreted in perturbative QCD.

The most relevant source for quark-antiquark (and also flavor) separation is provided by data from semi-inclusive DIS (SIDIS). Semi-inclusive measurements are usually performed at much lower scales than for  $e^+e^-$  annihilation. The inclusion of SIDIS data in global fits allows for a wider coverage in the evolution of the fragmentation functions, resulting at the same time in a stringent test of the universality of these distributions. Charged-hadron production data in hadronic collisions also presents a sensitivity on (anti-)quark fragmentation functions.

The gluon fragmentation function  $D_g(x)$  can be extracted, in principle, from the longitudinal fragmentation function  $F_L$  in Eq. (17.2), as the coefficient functions  $C_{L,i}$  for quarks and gluons are comparable at order  $\alpha_s$ . However at NLO, *i.e.*, including the  $\mathcal{O}(\alpha_s^2)$  coefficient functions  $C_{L,i}^{(2)}$  [23], quark fragmentation is dominant in  $F_L$  over a large part of the kinematic range, reducing the sensitivity on  $D_g$ . This distribution could be determined also analyzing the evolution of the fragmentation functions. This possibility is limited by the lack of sufficiently precise data at energy scales away from the  $Z$ -resonance and the dominance of the quark contributions and at medium and large values of  $x$ .

$D_g$  can also be deduced from the fragmentation of three-jet events in which the gluon jet is identified, for example, by tagging the other two jets with heavy quark decays. To leading order, the measured distributions of  $x = E_{\text{had}}/E_{\text{jet}}$  for particles in gluon jets can be identified directly with the gluon fragmentation functions  $D_g(x)$ . At higher orders the theoretical interpretation of this observable is ambiguous.

A direct constraint on  $D_g$  is provided by  $pp, p\bar{p} \rightarrow hX$  data. At variance with  $e^+e^-$  annihilation and SIDIS, for this process gluon fragmentation starts to contribute at the lowest order in the coupling constant, introducing a strong sensitivity on  $D_g$ . At large  $x \gtrsim 0.5$ , where information from  $e^+e^-$  is sparse, data from hadronic colliders facilitate significantly improved extractions of  $D_g$  [93,94].

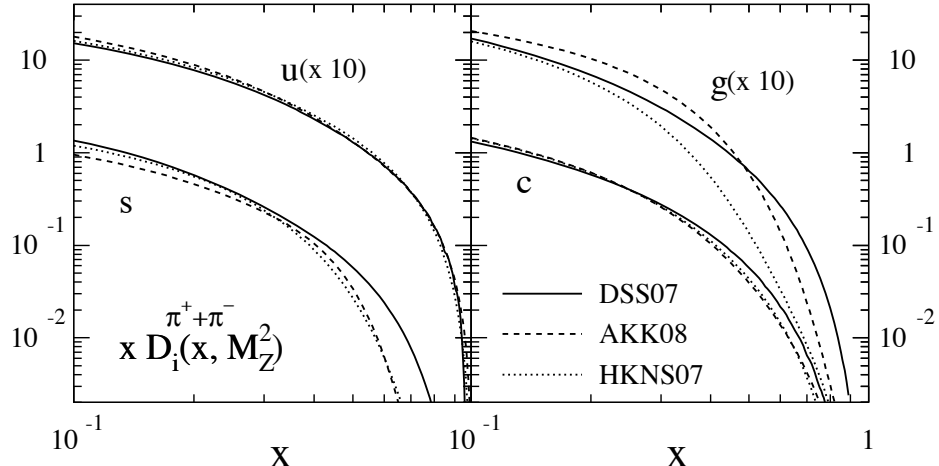


**Figure 17.6:** Comparison of up, strange, charm and gluon NLO fragmentation functions for  $\pi^+ + \pi^-$  at the mass of the  $Z$ . The different lines correspond to the result of the most recent analyses performed in Refs. [93,94,98].

A comparison of recent fits of NLO fragmentation functions for  $\pi^+ + \pi^-$  obtained by

## 12 17. Fragmentation functions in $e^+e^-$ , $ep$ and $pp$ collisions

DSS07 [93], AKK08 [94] and HKNS07 [98] is shown in Fig. 17.6. Differences between the sets are large especially for the gluon fragmentation function over the full range of  $x$  and for the quark distribution at large momentum fractions. Those discrepancies can be considered as a first estimate of the present uncertainties involved in the extraction of the fragmentation functions. The differences are even larger for other species of hadrons like kaons and protons [93,94,98].

### 17.6. Identified particles in $e^+e^-$ and semi-inclusive DIS

A great wealth of measurements of  $e^+e^-$  fragmentation into identified particles exists. A collection of references for data on fragmentation into identified particles is given on Table 41.1. Representative of this body of data is Fig. 17.7 which shows fragmentation functions as the scaled momentum spectra of charged particles at several CM energies.

Quantitative results of studies of scaling violation in  $e^+e^-$  fragmentation have been reported in [6,38,101,102]. The values of  $\alpha_s$  obtained are consistent with the world average (see review on QCD in Section 9 of this *Review*).

Many studies have been made of identified particles produced in lepton-hadron scattering, although fewer particle species have been measured than in  $e^+e^-$  collisions. References [103–108] and [109–115] are representative of the data from fixed target and  $ep$  collider experiments, respectively.

QCD calculations performed at NLO provide an overall good description of the HERA data [50,51,55,110,116,117] for both SIDIS [118] and the hadron transverse momentum distribution [46] in the kinematic regions in which the calculations are predictive.

Fig. 17.8(a) compares lower-energy fixed-target and HERA data on strangeness production, showing that the HERA spectra have substantially increased multiplicities, albeit with insufficient statistical precision to study scaling violations. The fixed-target data show that the  $\Lambda$  rate substantially exceeds the  $\bar{\Lambda}$  rate in the remnant region, owing to the conserved baryon number from the baryon target. Fig. 17.8(b) shows neutral and charged pion fragmentation functions  $1/N \cdot dn/dz$ , where  $z$  is defined as the ratio of the pion energy to that of the exchanged boson, both measured in the laboratory frame. Results are shown from HERMES and the EMC experiments, where HERMES data have been evolved with NLO QCD to  $\langle Q^2 \rangle = 25$  GeV $^2$  in order to be consistent with the EMC. Each of the experiments uses various kinematic cuts to ensure that the measured particles lie in the region which is expected to be associated with the struck quark. In the DIS kinematic regime accessed at these experiments, and over the range in  $z$  shown in Fig. 17.8, the  $z$  and  $x_F$  variables have similar values [47]. The precision data on identified particles can be used in the study of the quark flavor content of the proton [119].

Data on identified particle production can aid the investigation of the universality of jet fragmentation in  $e^+e^-$  and DIS. The strangeness suppression factor  $\gamma_s$ , as derived principally from tuning the Lund string model [84] within JETSET [85], is typically found to be around 0.3 in  $e^+e^-$  experiments [68], although values closer to 0.2 [120] have also been obtained. A number of measurements of so-called  $V^0$ -particles ( $K^0$ ,  $\Lambda^0$ ) and the relative rates of  $V^0$ 's and inclusively produced charged particles have been performed at HERA [109,111,115] and fixed target experiments [103]. These typically favour a stronger

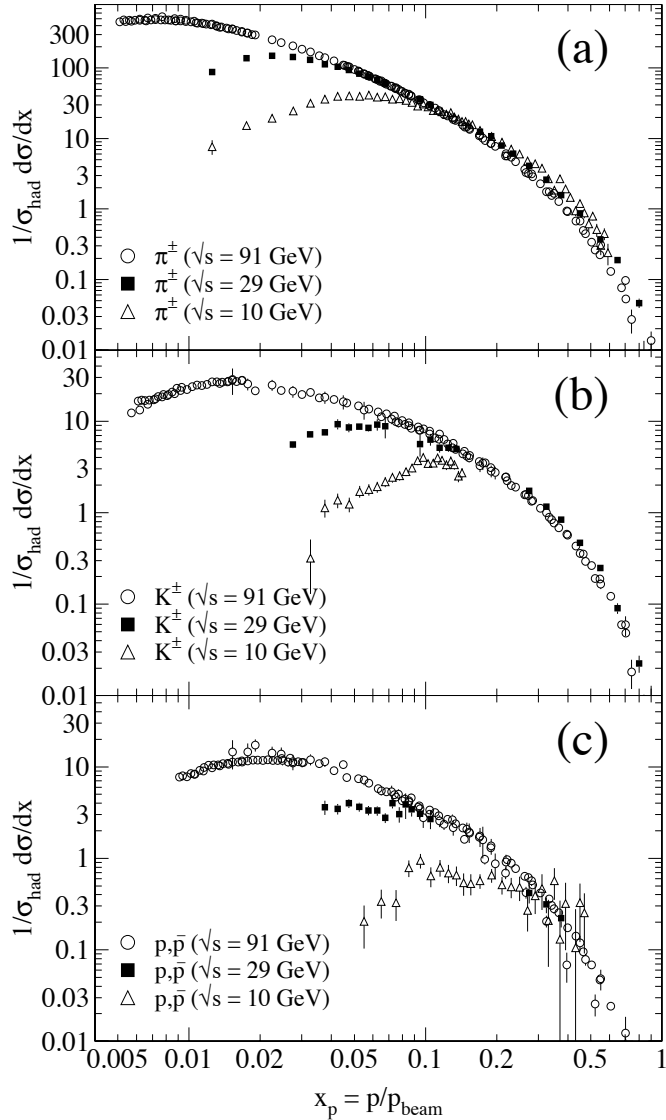


**Figure 17.7:** Scaled momentum spectra of (a)  $\pi^\pm$ , (b)  $K^\pm$ , and (c)  $p/\bar{p}$  at  $\sqrt{s} = 10, 29$ , and  $91$  GeV [37,41,78,100].

suppression ( $\gamma_s \approx 0.2$ ) than usually obtained from  $e^+e^-$  data although values close to 0.3 have also been obtained [121,122].

However, when comparing the description of QCD-based models for lepton-hadron interactions and  $e^+e^-$  collisions, it is important to note that the overall description by event generators of inclusively produced hadronic final states is more accurate in  $e^+e^-$  collisions than lepton-hadron interactions [123]. Predictions of particle rates in lepton-hadron scattering are affected by uncertainties in the modelling of the parton composition of the proton and photon, the extended target remnant, and initial and final state QCD radiation. Furthermore, the tuning of event generators for  $e^+e^-$  collisions is typically based on a larger set of parameters and uses more observables [68] than are used when optimizing models for lepton-hadron data [124].

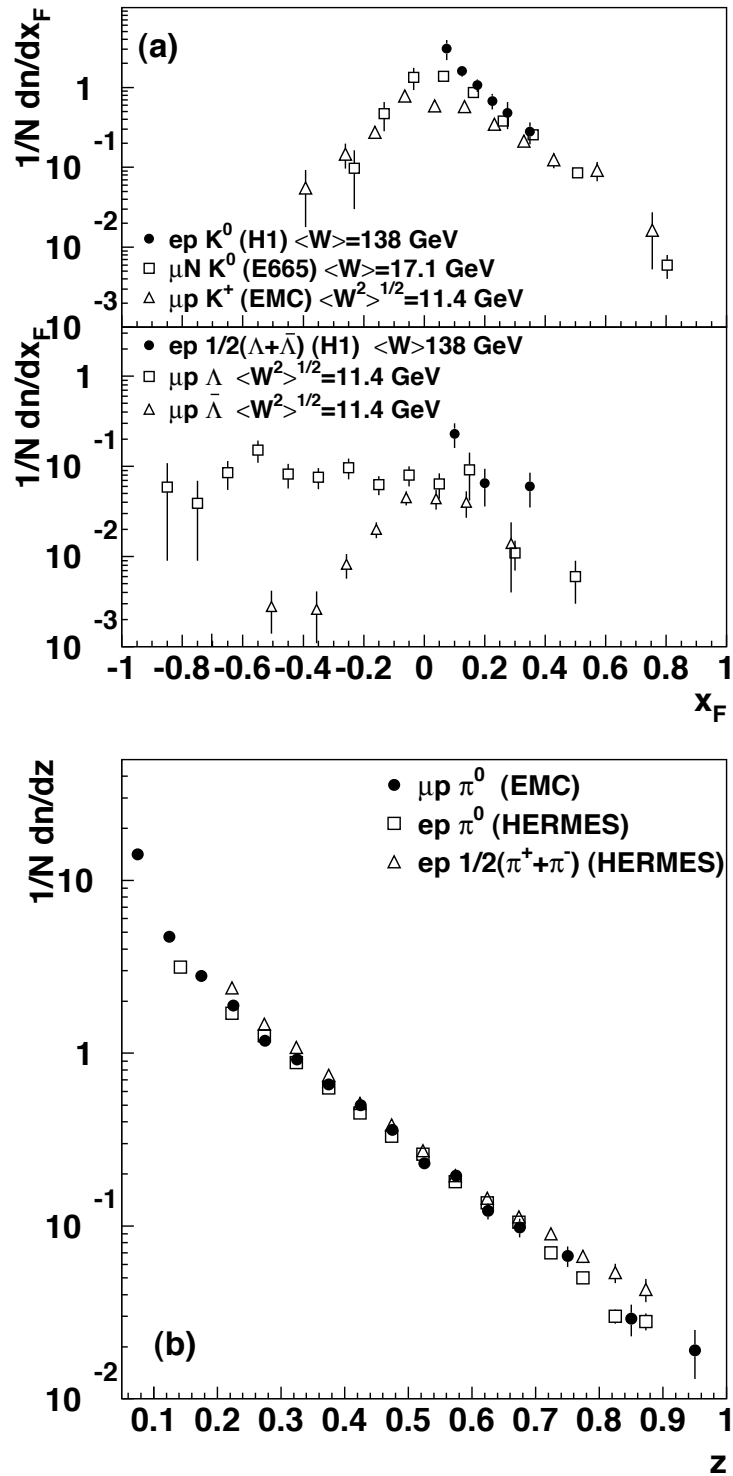


**Figure 17.8:** (a)  $1/N \cdot dn/dx_F$  for identified strange particles in DIS at various values of  $W$  [103,106,109]. (b)  $1/N \cdot dn/dz$  for measurements of pions from fixed-target DIS experiment [104,107,108].

### 17.7. Fragmentation in hadron-hadron collisions

An extensive set on high-transverse momentum ( $p_T$ ) single-inclusive hadron data has been collected in  $h_1 h_2 \rightarrow hX$  scattering processes, both at high energy colliders and fixed-target experiments [125–143]. Only the transverse momentum  $p_T$  is considered in hadron-hadron collisions because of lack of knowledge of the longitudinal momentum of the hard subprocess. Fig. 17.9 shows a compilation of neutral pion and charged hadron production data for energies in the range  $\sqrt{s} \approx 23 - 800$  GeV.

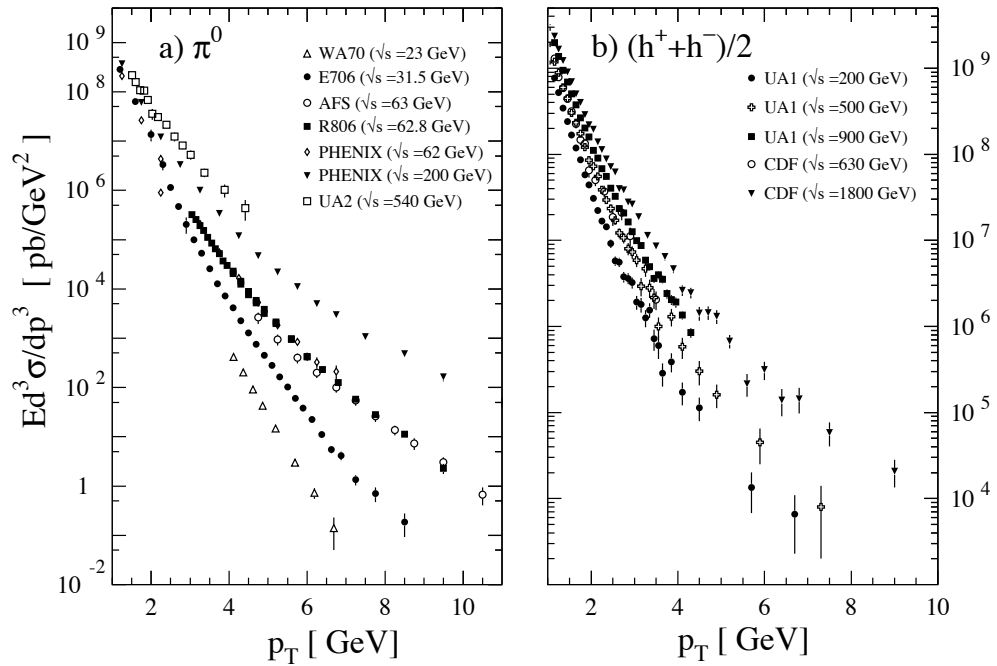


**Figure 17.9:** Selection of inclusive (a)  $\pi^0$  and (b) charged-hadron production data from  $pp$  [133,140–143] and  $p\bar{p}$  [125,128,131] collisions.

The differential cross-section for high-transverse momentum distributions has been computed to next-to-leading order accuracy in perturbative QCD [144]. NLO calculations yield a good description of the collider data, but significantly under-predict the cross-section for several fixed-target energy data sets [145,146]. Data collected at high energy colliders are either included in global fit analyses or used as a test for the universality of fragmentation functions.

Different strategies have been developed to ameliorate the theoretical description at fixed-target energies. A possible phenomenological approach involves the introduction of a non-perturbative intrinsic partonic transverse momentum [143,147,148]. From the perturbative side, the resummation of the dominant higher order corrections at threshold produces an enhancement of the theoretical calculation that significantly improves the description of the data [149].

Measurements of hadron production in longitudinally polarized  $pp$  collisions are used mainly in the determination of the polarized gluon distribution in the proton [150,151].

## 16 17. Fragmentation functions in $e^+e^-$ , $ep$ and $pp$ collisions

Hadron production provides a critical observable for probing the high energy-density matter produced in heavy-ion collisions. Measurements at colliders show a suppression of inclusive hadron yields at high transverse momentum for  $AA$  collisions compared to  $pp$  scattering, indicating the formation of a dense medium opaque to quark and gluons, see e.g. [152].

### 17.8. Spin-dependent fragmentation

Measurements of charged-hadron production in unpolarized lepton-hadron scattering provide a unique tool to perform a flavor-separation determination of polarized parton densities from DIS interactions with longitudinally polarized targets [153–157].

Polarized scattering presents the possibility to measure the spin transfer from the struck quark to the final hadron, and thus develop spin-dependent fragmentation functions [158,159]. Early measurements of the longitudinal spin transfer to Lambda hyperons have been presented in [160,161]. This process is also useful in the study of the quark transversity distribution [162], which describes the probability of finding a transversely polarized quark with its spin aligned or anti-aligned with the spin of a transversely polarized nucleon. The transversity function is chiral-odd, and therefore not accessible through measurements of inclusive lepton-hadron scattering. Semi-inclusive DIS, in which another chiral-odd observable may be involved, provides a valuable tool to probe transversity. The Collins fragmentation function [163] relates the transverse polarization of the quark to that of the final hadron. It is chiral-odd and naive T-odd, leading to a characteristic single spin asymmetry in the azimuthal angular distribution of the produced hadron in the hadron scattering plane. Azimuthal angular distributions in semi-inclusive DIS can also be produced by other processes requiring non-polarized fragmentation functions, like the Sivers mechanism [164].

A number of experiments have measured these asymmetries [165–173]. Collins and Sivers asymmetries have been shown experimentally to be non zero by the HERMES measurements on transversely polarized proton targets [166–168]. Independent information on the Collins function has been provided by the BELLE Collaboration [169–170]. Measurements performed by the COMPASS collaboration on deuteron targets show results compatible with zero for both asymmetries [171–173].

### 17.9. Heavy quark fragmentation

It was recognized very early [174] that a heavy flavored meson should retain a large fraction of the momentum of the primordial heavy quark, and therefore its fragmentation function should be much harder than that of a light hadron. In the limit of a very heavy quark, one expects the fragmentation function for a heavy quark to go into any heavy hadron to be peaked near  $x = 1$ .

When the heavy quark is produced at a momentum much larger than its mass, one expects important perturbative effects, enhanced by powers of the logarithm of the transverse momentum over the heavy quark mass, to intervene and modify the shape of the fragmentation function. In leading logarithmic order (*i.e.*, including all powers of  $\alpha_s \log m_Q/p_T$ ), the total (*i.e.*, summed over all hadron types) perturbative

fragmentation function is simply obtained by solving the leading evolution equation for fragmentation functions, Eq. (17.4), with the initial condition at a scale  $\mu^2 = m_Q^2$  given by  $D_Q(z, m_Q^2) = \delta(1 - z)$  and  $D_i(z, m_Q^2) = 0$  for  $i \neq Q$  (here  $D_i(z)$ , stands for the probability to produce a heavy quark  $Q$  from parton  $i$  with a fraction  $z$  of the parton momentum).

Several extensions of the leading logarithmic result have appeared in the literature. Next-to-leading-log (NLL) order results for the perturbative heavy quark fragmentation function have been obtained in [175]. The resummation of the dominant logarithmic contributions at large  $z$  was performed in [42] to next-to-leading-log accuracy. Fixed-order calculations of the fragmentation function at order  $\alpha_s^2$  in  $e^+e^-$  annihilation have appeared in [176] while the initial condition for the perturbative heavy quark fragmentation function has been extended to NNLO in [177].

Inclusion of non-perturbative effects in the calculation of the heavy-quark fragmentation function is done by convoluting the perturbative result with a phenomenological non-perturbative form [178–183], see also section 17.8 of [184]. The parameters entering the non-perturbative forms are fitted together with some model of hard radiation, which can be either a shower Monte Carlo, a leading-log or NLL calculation (which may or may not include Sudakov resummation), or a fixed order calculation [176,185].

A more conventional approach [186] involves the introduction of a unique set of heavy quark fragmentation functions of non-perturbative nature that obey the usual massless evolution equations in Eq. (17.4). Finite mass terms of the form  $(m_Q/p_T)^n$  are kept in the corresponding short distance coefficient function for each scattering process. Within this approach, the initial condition for the perturbative fragmentation function provides the term needed to define the correct subtraction scheme to match the massless limit for the coefficient function (see e.g. [187]). Such implementation is in line with the variable flavor number scheme introduced for parton distributions functions, as described in Section 16 of this *Review*.

High statistics data for charmed mesons production near the  $\Upsilon$  resonance (excluding decay products of  $B$  mesons) have been published [188,189]. They include results for  $D$  and  $D^*$ ,  $D_s$  (see also [190,191]) and  $\Lambda_c$ . Shown in Fig. 17.10(a) are the CLEO and BELLE inclusive cross-sections times branching ratio  $\mathcal{B}$ ,  $s \cdot \mathcal{B} d\sigma/dx_p$ , for the production of  $D^0$  and  $D^{*+}$ . The variable  $x_p$  approximates the light-cone momentum fraction  $z$ , but is not identical to it. The two measurements are consistent with each other.

The branching ratio  $\mathcal{B}$  represents  $D^0 \rightarrow K^-\pi^+$  for the  $D^0$  results and for the  $D^{*+}$  the product branching fraction:  $D^{*+} \rightarrow D^0\pi^+$ ,  $D^0 \rightarrow K^-\pi^+$ . Given the high precision of CLEO's and BELLE's data, a superposition of different parametric forms for the non-perturbative contribution is needed to obtain a good fit [21]. Older studies are reported in Refs. [192–194]. Charmed meson spectra on the  $Z$  peak have been published by OPAL and ALEPH [90,195].

Charm quark production has also been extensively studied at HERA by the H1 and ZEUS collaborations. Measurements have been made of  $D^{*\pm}$ ,  $D^\pm$ , and  $D_s^\pm$  mesons; see, for example, Refs. [196,197]. The production of the  $\Lambda_c$  baryon has also been studied [198].

Experimental studies of the fragmentation function for  $b$  quarks, shown in Fig. 17.10(b),

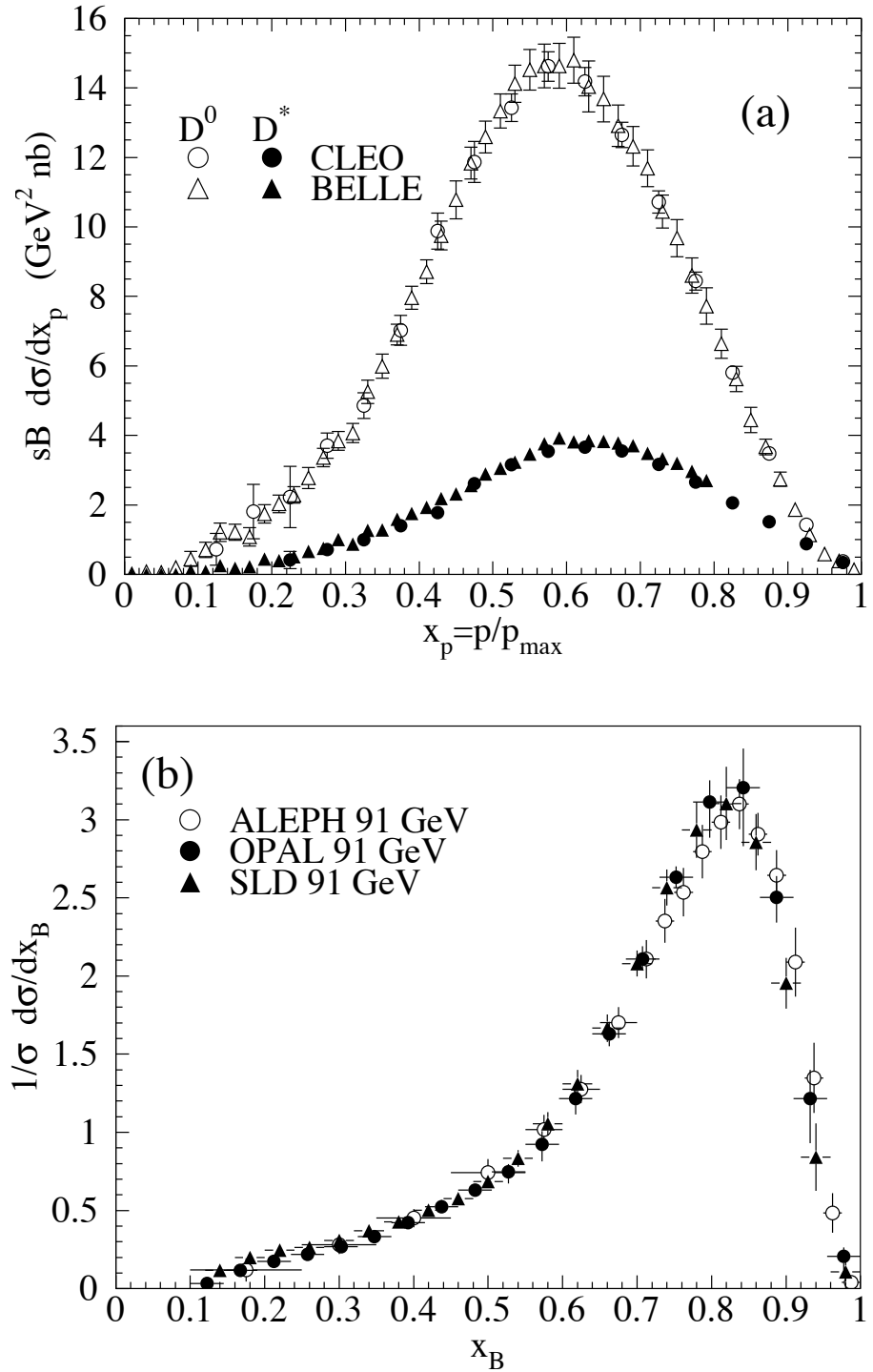


**Figure 17.10:** (a) Efficiency-corrected inclusive cross-section measurements for the production of  $D^0$  and  $D^{*+}$  in  $e^+e^-$  measurements at  $\sqrt{s} \approx 10.6$  GeV, excluding  $B$  decay products [188,189]. (b) Measured  $e^+e^-$  fragmentation function of  $b$  quarks into  $B$  hadrons at  $\sqrt{s} \approx 91$  GeV [200].

have been performed at LEP and SLD [199–201]. Commonly used methods identify the  $B$  meson through its semileptonic decay or based upon tracks emerging from the  $B$  secondary vertex. The studies in [200] fit the  $B$  spectrum using a Monte Carlo shower model supplemented with non-perturbative fragmentation functions yielding consistent results.

The experiments measure primarily the spectrum of  $B$  mesons. This defines a fragmentation function which includes the effect of the decay of higher mass excitations, like the  $B^*$  and  $B^{**}$ . In the literature, there is sometimes ambiguity in what is defined to be the bottom fragmentation function. Instead of using what is directly measured (*i.e.*, the  $B$  meson spectrum) corrections are applied to account for  $B^*$  or  $B^{**}$  production in some cases. For a more detailed discussion see section 17.8 of [184].

Heavy-flavor production in  $e^+e^-$  collisions is the primary source of information for the role of fragmentation effects in heavy-flavor production in hadron-hadron and lepton-hadron collisions. The QCD calculations tend to underestimate the data in certain regions of phase space. The discrepancy observed between theoretical calculations and the measured  $B$  meson spectrum at the hadron colliders [202] is substantially reduced when a more refined use of information on heavy flavor production from  $e^+e^-$  data is made [203] and when up-to-date parton distributions and strong coupling constant values are considered [204].

Both bottomed- and charmed-mesons spectra have been measured at the Tevatron with unprecedented accuracy [205]. The measured spectra are in good agreement with QCD calculations (including non-perturbative fragmentation effects inferred from  $e^+e^-$  data [206]), no longer supporting the previously reported discrepancies [202].

The HERA collaborations have produced a number of measurements of beauty production; see, for example, Refs. [196,207–209]. As for the Tevatron data, the HERA results are described well by QCD-based calculations using fragmentation models optimised with  $e^+e^-$  data.

Besides degrading the fragmentation function by gluon radiation, QCD evolution can also generate soft heavy quarks, increasing in the small  $x$  region as  $\sqrt{s}$  increases. Several theoretical studies are available on the issue of how often  $b\bar{b}$  or  $c\bar{c}$  pairs are produced indirectly, via a gluon splitting mechanism [210–212]. Experimental results from studies on charm and bottom production via gluon splitting, given in [195,213–217], yield weighted averages of  $\overline{n}_{g \rightarrow c\bar{c}} = 3.05 \pm 0.45\%$  and  $\overline{n}_{g \rightarrow b\bar{b}} = 0.277 \pm 0.072\%$ , respectively.

## References:

1. G. Altarelli, Phys. Reports **81**, 1 (1982).
2. R.K. Ellis *et al.*, *QCD and Collider Physics*, Cambridge University Press (1996).
3. S. Albino *et al.*, arXiv:0804.2021 [hep-ph].
4. F. Arleo, Eur. Phys. J. **C61**, 603 (2009).
5. P. Nason and B.R. Webber, Nucl. Phys. **B421**, 473 (1994); Erratum *ibid.* **B480**, 755 (1996).
6. ALEPH Collab.: D. Barate *et al.*, Phys. Lett. **B357**, 487 (1995); Erratum *ibid.*, **B364**, 247 (1995).
7. OPAL Collab.: R. Akers *et al.*, Z. Phys. **C86**, 203 (1995).

## 20 17. Fragmentation functions in $e^+e^-$ , $ep$ and $pp$ collisions

8. DELPHI Collab.: P. Abreu *et al.*, Eur. Phys. J. **C6**, 19 (1999).
9. W. Kittel and E.A. De Wolf, *Soft Multihadron Dynamics*, World Scientific (2005).
10. H.F. Jones, Nuovo Cimento **40A**, 1018 (1965);  
K.H. Streng *et al.*, Z. Phys. **C2**, 237 (1979).
11. V.N. Gribov and L.N. Lipatov, Sov. J. Nucl. Phys. **15**, 438 (1972);  
V.N. Gribov and L.N. Lipatov, Sov. J. Nucl. Phys. **15**, 675 (1972);  
G. Altarelli and G. Parisi, Nucl. Phys. **B126**, 298 (1977);  
Yu.L. Dokshitzer, Sov. Phys. JETP Lett. **46**, 641 (1977).
12. H. Georgi and H.D. Politzer, Nucl. Phys. **B136**, 445 (1978);  
J.F. Owens, Phys. Lett. **B76**, 85 (1978);  
T. Uematsu, Phys. Lett. **B79**, 97 (1978).
13. G. Curci *et al.*, Nucl. Phys. **B175**, 27 (1980).
14. W. Furmanski and R. Petronzio, Phys. Lett. **97B**, 437 (1980).
15. E.G. Floratos *et al.*, Nucl. Phys. **B192**, 417 (1981);  
T. Munehisa *et al.*, Prog. Theor. Phys. **67**, 609 (1982).
16. J. Kalinowski *et al.*, Nucl. Phys. **B181**, 221 (1981);  
J. Kalinowski *et al.*, Nucl. Phys. **B181**, 253 (1981).
17. M. Stratmann and W. Vogelsang, Nucl. Phys. **B496**, 41 (1997).
18. Yu.L. Dokshitzer *et al.*, Phys. Lett. **B634**, 504 (2006).
19. A. Mitov *et al.*, Phys. Lett. **B638**, 61 (2006).
20. S. Moch and A. Vogt, Phys. Lett. **B659**, 290 (2008).
21. M. Cacciari *et al.*, JHEP **0604**, 006 (2006).
22. G. Altarelli *et al.*, Nucl. Phys. **B160**, 301 (1979);  
R. Baier and K. Fey, Z. Phys. **C2**, 339 (1979).
23. P.J. Rijken and W.L. van Neerven, Phys. Lett. **B386**, 422 (1996);  
P.J. Rijken and W.L. van Neerven, Phys. Lett. **B392**, 207 (1997);  
P.J. Rijken and W.L. van Neerven, Nucl. Phys. **B487**, 233 (1997).
24. A. Mitov and S. Moch, Nucl. Phys. **B751**, 18 (2006).
25. ALEPH Collab.: D. Buskulic *et al.*, Z. Phys. **C73**, 409 (1997).
26. ALEPH Collab.: E. Barate *et al.*, Phys. Reports **294**, 1 (1998).
27. L3 Collab.: B. Adeva *et al.*, Phys. Lett. **B259**, 199 (1991).
28. AMY Collab.: Y.K. Li *et al.*, Phys. Rev. **D41**, 2675 (1990).
29. HRS Collab.: D. Bender *et al.*, Phys. Rev. **D31**, 1 (1984).
30. MARK II Collab.: G.S. Abrams *et al.*, Phys. Rev. Lett. **64**, 1334 (1990).
31. MARK II Collab.: A. Petersen *et al.*, Phys. Rev. **D37**, 1 (1988).
32. OPAL Collab.: R. Akers *et al.*, Z. Phys. **C72**, 191 (1996).
33. OPAL Collab.: K. Ackerstaff *et al.*, Z. Phys. **C75**, 193 (1997).
34. OPAL Collab.: K. Ackerstaff *et al.*, Eur. Phys. J. **C7**, 369 (1998).
35. OPAL Collab.: G. Abbiendi *et al.*, Eur. Phys. J. **C16**, 185 (2000);  
OPAL Collab.: G. Abbiendi *et al.*, Eur. Phys. J. **C27**, 467 (2003).
36. OPAL Collab.: G. Abbiendi *et al.*, Eur. Phys. J. **C37**, 25 (2004).
37. SLD Collab.: K. Abe *et al.*, Phys. Rev. **D69**, 072003 (2004).
38. DELPHI Collab.: P. Abreu *et al.*, Phys. Lett. **B398**, 194 (1997).
39. TASSO Collab.: R. Brandelik *et al.*, Phys. Lett. **B114**, 65 (1982).

40. TASSO Collab.: W. Braunschweig *et al.*, Z. Phys. **C47**, 187 (1990).
41. TPC Collab.: H. Aihara *et al.*, Phys. Rev. Lett. **61**, 1263 (1988).
42. M. Cacciari and S. Catani, Nucl. Phys. **B617**, 253 (2001).
43. J. Blümlein and V. Ravindran, Phys. Lett. **B640**, 40 (2006).
44. S. Moch and A. Vogt, Phys. Lett. **B680**, 239 (2009).
45. S. Moch and A. Vogt, JHEP **0911**, 099 (2009).
46. P. Aurenche *et al.*, Eur. Phys. J. **C34**, 277 (2004);  
A. Daleo *et al.*, Phys. Rev. **D71**, 034013 (2005);  
B.A. Kniehl *et al.*, Nucl. Phys. **B711**, 345 (2005);  
Erratum *ibid.* **B720**, 231 (2005).
47. E665 Collab.: M.R. Adams *et al.*, Phys. Lett. **B272**, 163 (1991).
48. EMC Collab.: M. Arneodo *et al.*, Z. Phys. **C35**, 417 (1987).
49. H1 Collab.: I. Abt *et al.*, Z. Phys. **C63**, 377 (1994).
50. ZEUS Collab.: M. Derrick *et al.*, Z. Phys. **C70**, 1 (1996).
51. ZEUS Collab.: J. Breitweg *et al.*, Phys. Lett. **B414**, 428 (1997).
52. H1 Collab.: S. Aid *et al.*, Nucl. Phys. **B445**, 3 (1995).
53. ZEUS Collab.: M. Derrick *et al.*, Z. Phys. **C67**, 93 (1995).
54. H1 Collab.: C. Adloff *et al.*, Nucl. Phys. **B504**, 3 (1997).
55. ZEUS Collab.: J. Breitweg *et al.*, Eur. Phys. J. **C11**, 251 (1999).
56. H1 Collab.: F.D. Aaron *et al.*, Phys. Lett. **B654**, 148 (2007).
57. DELPHI Collab.: P. Abreu *et al.*, Phys. Lett. **B311**, 408 (1993).
58. MARK II Collab.: J.F. Patrick *et al.*, Phys. Rev. Lett. **49**, 1232, (1982).
59. ZEUS Collab.: S. Chekanov *et al.*, JHEP **0608**, 061 (2008).
60. A.H. Mueller, Phys. Lett. **B104**, 161 (1981).
61. A. Bassetto *et al.*, Nucl. Phys. **B207**, 189 (1982).
62. Yu.L. Dokshitzer *et al.*, Z. Phys. **C15**, 324 (1982).
63. A.H. Mueller, Nucl. Phys. **B213**, 85 (1983);  
Erratum in *ibid.* **B241**, 141 (196).
64. Yu.L. Dokshitzer *et al.*, Int. J. Mod. Phys. **A7**, 1875 (1992).
65. Yu.L. Dokshitzer *et al.*, *Basics of Perturbative QCD*, Editions Frontières (1991).
66. V.A. Khoze and W. Ochs, Int. J. Mod. Phys. **A12**, 2949 (1997).
67. C.P. Fong and B.R. Webber, Nucl. Phys. **B355**, 54 (1992).
68. DELPHI Collab.: P. Abreu *et al.*, Z. Phys. **C73**, 11 (1996).
69. DELPHI Collab.: P. Abreu *et al.*, Z. Phys. **C73**, 229 (1997).
70. L3 Collab.: P. Achard *et al.*, Phys. Reports **399**, 71 (2004).
71. TOPAZ Collab.: R. Itoh *et al.*, Phys. Lett. **B345**, 335 (1995).
72. TASSO Collab.: W. Braunschweig *et al.*, Z. Phys. **C22**, 307 (1990).
73. OPAL Collab.: M.Z. Akrawy *et al.*, Phys. Lett. **B247**, 617 (1990).
74. BES Collab.: J.Z. Bai *et al.*, Phys. Rev. **D69**, 072002 (2004).
75. ALEPH Collab.: D. Buskulic *et al.*, Z. Phys. **C55**, 209 (1992).
76. ALEPH Collab.: A. Heister *et al.*, Eur. Phys. J. **C35**, 457 (2004).
77. DELPHI Collab.: P. Abreu *et al.*, Phys. Lett. **B275**, 231 (1992).
78. DELPHI Collab.: P. Abreu *et al.*, Eur. Phys. J. **C5**, 585 (1998).
79. DELPHI Collab.: P. Abreu *et al.*, Phys. Lett. **B459**, 397 (1999).

## 22 17. Fragmentation functions in $e^+e^-$ , $ep$ and $pp$ collisions

80. L3 Collab.: M. Acciarri *et al.*, Phys. Lett. **B444**, 569 (1998).
81. TPC/TWO-GAMMA Collab.: H. Aihara *et al.*, LBL 23737.
82. S. Höche *et al.*, arXiv:hep-ph/0602031;  
J. Alwall *et al.*, Eur. Phys. J. **C53**, 473 (2008);  
S. Mrenna and P. Richardson, JHEP **0405**, 040 (2004).
83. X. Artru and G. Mennessier, Nucl. Phys. **B70**, 93 (1974).
84. B. Andersson *et al.*, Phys. Reports **97**, 31 (1983).
85. T. Sjöstrand and M. Bengtsson, Comp. Phys. Comm. **43**, 367 (1987);  
T. Sjöstrand, Comp. Phys. Comm. **82**, 74 (1994).
86. T. Sjöstrand, S. Mrenna, P. Skands, JHEP **0605**, 026 (2006);  
T. Sjöstrand, S. Mrenna, P. Skands, Comp. Phys. Comm. **178**, 852 (2008).
87. S. Chun and C. Buchanan, Phys. Reports **292**, 239 (1998).
88. G. Marchesini *et al.*, Comp. Phys. Comm. **67**, 465 (1992);  
G. Corcella *et al.*, JHEP **0101**, 010 (2001);  
M. Bähr *et al.*, Eur. Phys. J. **C58**, 639 (2008).
89. T. Gleisberg *et al.*, JHEP **0902**, 007 (2009).
90. OPAL Collab.: G. Alexander *et al.*, Z. Phys. **C69**, 543 (1996).
91. M. Schmelling, Phys. Scripta **51**, 683 (1995).
92. D. Amati and G. Veneziano, Phys. Lett. **B83**, 87 (1979).
93. D. de Florian *et al.*, Phys. Rev. **D76**, 074033 (2007);  
D. de Florian *et al.*, Phys. Rev. **D75**, 114010 (2007).
94. S. Albino *et al.*, Nucl. Phys. **B803**, 42 (2008).
95. S. Kretzer *et al.*, Eur. Phys. J. **C22**, 269 (2001).
96. S. Kretzer, Phys. Rev. **D62**, 054001 (2000).
97. L. Bourhis *et al.*, Eur. Phys. J. **C19**, 89 (2001).
98. M. Hirai *et al.*, Phys. Rev. **D75**, 094009 (2007).
99. ALEPH Collab.: R. Barate *et al.*, Eur. Phys. J. **C17**, 1 (2000);  
OPAL Collab.: R. Akers *et al.*, Z. Phys. **C68**, 179 (1995);  
OPAL Collab.: G. Abbiendi *et al.*, Eur. Phys. J. **C11**, 217 (1999).
100. ALEPH Collab.: D. Buskulic *et al.*, Z. Phys. **C66**, 355 (1995);  
ARGUS Collab.: H. Albrecht *et al.*, Z. Phys. **C44**, 547 (1989);  
OPAL Collab.: R. Akers *et al.*, Z. Phys. **C63**, 181 (1994);  
SLD Collab.: K. Abe *et al.*, Phys. Rev. **D59**, 052001 (1999).
101. DELPHI Collab.: P. Abreu *et al.*, Eur. Phys. J. **C13**, 573 (2000).
102. B.A. Kniehl *et al.*, Phys. Rev. Lett. **85**, 5288 (2000).
103. E665 Collab.: M.R. Adams *et al.*, Z. Phys. **C61**, 539 (1994).
104. EMC Collab.: J.J. Aubert *et al.*, Z. Phys. **C18**, 189 (1983);  
EMC Collab.: M. Arneodo *et al.*, Phys. Lett. **B150**, 458 (1985).
105. EMC Collab.: M. Arneodo *et al.*, Z. Phys. **C33**, 167 (1986).
106. EMC Collab.: M. Arneodo *et al.*, Z. Phys. **C34**, 283 (1987).
107. HERMES Collab.: A. Airapetian *et al.*, Eur. Phys. J. **C21**, 599 (2001).
108. T.P. McPharlin *et al.*, Phys. Lett. **B90**, 479 (1980).
109. H1 Collab.: S. Aid *et al.*, Nucl. Phys. **B480**, 3 (1996).

110. H1 Collab.: C. Adloff *et al.*, Eur. Phys. J. **C18**, 293 (2000);  
H1 Collab.: A. Aktas *et al.*, Eur. Phys. J. **C36**, 413 (2004).
111. ZEUS Collab.: M. Derrick *et al.*, Z. Phys. **C68**, 29 (1995);  
ZEUS Collab.: J. Breitweg *et al.*, Eur. Phys. J. **C2**, 77 (1998).
112. ZEUS Collab.: S. Chekanov *et al.*, Phys. Lett. **B553**, 141 (2003).
113. ZEUS Collab.: S. Chekanov *et al.*, Nucl. Phys. **B786**, 181 (2007).
114. H1 Collab.: F. D. Aaron *et al.*, Eur. Phys. J. **C61**, 185 (2009).
115. H1 Collab.: F. D. Aaron *et al.*, Phys. Lett. **B673**, 119 (2009).
116. P. Dixon *et al.*, J. Phys. **G25**, 1453 (1999).
117. H1 Collab.: C. Adloff *et al.*, Phys. Lett. **B462**, 440 (1999).
118. D. Graudenz, Fortsch. Phys. **45**, 629 (1997).
119. S. Albino *et al.*, Phys. Rev. **D75**, 034018 (2007).
120. OPAL Collab.: P.D. Acton *et al.*, Phys. Lett. **B305**, 407 (1993).
121. E632 Collab.: D. DeProspo *et al.*, Phys. Rev. **D50**, 6691 (1994).
122. ZEUS Collab.: S. Chekanov *et al.*, Eur. Phys. J. **C51**, 1 (2007).
123. G. Grindhammer *et al.*, in: *Proceedings of the Workshop on Monte Carlo Generators for HERA Physics*, Hamburg, Germany, 1998/1999.
124. N. Brook *et al.*, in: *Proceedings of the Workshop for Future HERA Physics at HERA*, Hamburg, Germany, 1996.
125. CDF Collab.: F. Abe *et al.*, Phys. Rev. Lett. **61**, 1819 (1988).
126. CDF Collab.: D. E. Acosta *et al.*, Phys. Rev. **D72**, 052001 (2005).
127. UA1 Collab.: G. Arnison *et al.*, Phys. Lett. **B118**, 167 (1982).
128. UA1 Collab.: C. Albajar *et al.*, Nucl. Phys. **B335**, 261 (1990).
129. UA1 Collab.: G. Bocquet *et al.*, Phys. Lett. **B366**, 434 (1996).
130. UA2 Collab.: M. Banner *et al.*, Phys. Lett. **B122**, 322 (1983).
131. UA2 Collab.: M. Banner *et al.*, Phys. Lett. **B115**, 59 (1982).
132. UA2 Collab.: M. Banner *et al.*, Z. Phys. **C27**, 329 (1985).
133. PHENIX Collab.: S. S. Adler *et al.*, Phys. Rev. Lett. **91**, 241803 (2003).
134. BRAHMS Collab.: I. Arsene *et al.*, Phys. Rev. Lett. **98**, 252001 (2007).
135. STAR Collab.: J. Adams *et al.*, Phys. Lett. **B637**, 161 (2006).
136. STAR Collab.: J. Adams *et al.*, Phys. Rev. Lett. **97**, 152302 (2006).
137. STAR Collab.: B. I. Abelev *et al.*, Phys. Rev. **C75**, 064901 (2007).
138. E706 Collab.: L. Apanasevich *et al.*, Phys. Rev. Lett. **81**, 2642 (1998).
139. UA6 Collab.: G. Ballocchi *et al.*, Phys. Lett. **B436**, 222 (1998).
140. WA70 Collab.: M. Bonesini *et al.*, Z. Phys. **C38**, 371 (1988).
141. AFS Collab.: E. Anassontzis *et al.*, Sov. J. Nucl. Phys. **51**, 836 (1990).
142. R806 Collab.: C. Kourkoumelis *et al.*, Z. Phys. **C5**, 95 (1980).
143. E706 Collab.: L. Apanasevich *et al.*, Phys. Rev. **D68**, 052001 (2003).
144. F. Aversa *et al.*, Nucl. Phys. **B327**, 105 (1989);  
D. de Florian, Phys. Rev. **D67**, 054004 (2003);  
B. Jager *et al.*, Phys. Rev. **D67**, 054005 (2003).
145. U. Baur *et al.*, arXiv:hep-ph/0005226.
146. P. Aurenche, *et al.*, Eur. Phys. J. **C13**, 347 (2000).
147. L. Apanasevich *et al.*, Phys. Rev. **D59**, 074007 (1999).

## 24 17. Fragmentation functions in $e^+e^-$ , $ep$ and $pp$ collisions

148. U. D'Alesio and F. Murgia, Phys. Rev. **D70**, 074009 (2004).
149. D. de Florian and W. Vogelsang, Phys. Rev. **D71**, 114004 (2005).
150. PHENIX Collab.: A. Adare *et al.*, Phys. Rev. **D76**, 051106 (2007).
151. PHENIX Collab.: A. Adare *et al.*, Phys. Rev. **D79**, 012003 (2009).
152. PHENIX Collab.: K. Adcox *et al.*, Phys. Rev. Lett. **88**, 022301 (2002); STAR Collab.: C. Adler *et al.*, Phys. Rev. Lett. **90**, 082302 (2003).
153. COMPASS Collab.: M. Alekseev *et al.*, Phys. Lett. **B660**, 458, (2008).
154. HERMES Collab.: A. Airapetian *et al.*, Phys. Rev. **D71**, 012003 (2005).
155. SMC Collab.: B. Adeva *et al.*, Phys. Lett. **B420**, 180 (1998).
156. HERMES Collab.: A. Airapetian *et al.*, Phys. Lett. **B666**, 446 (2008).
157. D. de Florian *et al.*, Phys. Rev. Lett. **101**, 072001 (2008).
158. P.J. Mulders and R.D. Tangerman, Nucl. Phys. **B461**, 197 (1996); Erratum *ibid.*, **B484**, 538 (1997).
159. R. Jacob, Nucl. Phys. **A711**, 35 (2002).
160. COMPASS Collab.: M. Alekseev *et al.*, Eur. Phys. J. **C64**, 171 (2009).
161. HERMES Collab.: A. Airapetian *et al.*, Phys. Rev. **D74**, 072004 (2006).
162. J.P. Ralston and D.E. Soper, Nucl. Phys. **B152**, 109 (1979).
163. J. Collins, Nucl. Phys. **B396**, 161 (1993).
164. D. Sivers, Phys. Rev. **D43**, 261 (1991).
165. CLAS Collab.: H. Avakian *et al.*, Phys. Rev. **D69**, 112004 (2004).
166. HERMES Collab.: A. Airapetian *et al.*, Phys. Rev. Lett. **84**, 4047 (2000).
167. HERMES Collab.: A. Airapetian *et al.*, Phys. Rev. **D64**, 097101 (2001).
168. HERMES Collab.: A. Airapetian *et al.*, Phys. Rev. Lett. **94**, 012002 (2005).
169. BELLE Collab.: K. Abe *et al.*, Phys. Rev. Lett. **96**, 232002 (2006).
170. BELLE Collab.: K. Abe *et al.*, Phys. Rev. **D78**, 032011 (2008).
171. COMPASS Collab.: V.Y Alexakhin *et al.*, Phys. Rev. Lett. **94**, 202002 (2005).
172. COMPASS Collab.: V.Y Alexakhin *et al.*, Nucl. Phys. **B765**, 31 (2007).
173. COMPASS Collab.: M. Alekseev *et al.*, Phys. Lett. **B673**, 127 (2009).
174. V.A. Khoze *et al.*, *Proceedings, Conference on High-Energy Physics, Tbilisi 1976*; J.D. Bjorken, Phys. Rev. **D17**, 171 (1978).
175. B. Mele and P. Nason, Phys. Lett. **B245**, 635 (1990);  
B. Mele and P. Nason, Nucl. Phys. **B361**, 626 (1991).
176. P. Nason and C. Oleari, Phys. Lett. **B418**, 199 (1998);  
P. Nason and C. Oleari, Phys. Lett. **B447**, 327 (1999);  
P. Nason and C. Oleari, Nucl. Phys. **B565**, 245 (2000).
177. K. Melnikov and A. Mitov, Phys. Rev. **D70**, 034027 (2004).
178. C. Peterson *et al.*, Phys. Rev. **D27**, 105 (1983).
179. V.G. Kartvelishvili *et al.*, Phys. Lett. **B78**, 615 (1978).
180. P. Collins and T. Spiller, J. Phys. **G11**, 1289 (1985).
181. G. Colangelo and P. Nason, Phys. Lett. **B285**, 167 (1992).
182. M.G. Bowler, Z. Phys. **C11**, 169 (1981).
183. E. Braaten *et al.*, Phys. Rev. **D51**, 4819 (1995).
184. Particle Data Group: C. Amsler *et al.*, Phys. Lett. **B667**, 1 (2008).
185. J. Chrin, Z. Phys. **C36**, 163 (1987).

186. J. Collins, Phys. Rev. **D58**, 094002 (1998).
187. B.A. Kniehl *et al.*, Eur. Phys. J. **C41**, 199 (2005).
188. CLEO Collab.: M. Artuso *et al.*, Phys. Rev. **D70**, 112001 (2004).
189. BELLE Collab.: R. Seuster *et al.*, Phys. Rev. **D73**, 032002 (2006).
190. CLEO Collab.: R.A. Briere *et al.*, Phys. Rev. **D62**, 112003 (2000).
191. BABAR Collab.: B. Aubert *et al.*, Phys. Rev. **D65**, 091104 (2002).
192. CLEO Collab.: D. Bortoletto *et al.*, Phys. Rev. **D37**, 1719 (1988).
193. ARGUS Collab.: H. Albrecht *et al.*, Z. Phys. **C52**, 353 (1991).
194. ARGUS Collab.: H. Albrecht *et al.*, Z. Phys. **C54**, 1 (1992).
195. ALEPH Collab.: R. Barate *et al.*, Phys. Lett. **B561**, 213 (2003).
196. H1 Collab.: F.D. Aaron *et al.*, Eur. Phys. J. **C65**, 89 (2010).
197. ZEUS Collab.: S. Chekanov *et al.*, JHEP **0707**, 074 (2007);  
ZEUS Collab.: S. Chekanov *et al.*, JHEP **0904**, 82 (2009);  
ZEUS Collab.: S. Chekanov *et al.*, Eur. Phys. J. **C63**, 171 (2009);  
H1 Collab.: A. Aktas *et al.*, Eur. Phys. J. **C51**, 271 (2007);  
H1 Collab.: F. D. Aaron *et al.*, Eur. Phys. J. **C59**, 589 (2009).
198. ZEUS Collab.: S. Chekanov *et al.*, Eur. Phys. J. **C44**, 351 (2005).
199. ALEPH Collab.: D. Buskulic *et al.*, Phys. Lett. **B357**, 699 (1995).
200. ALEPH Collab.: A. Heister *et al.*, Phys. Lett. **B512**, 30 (2001);  
OPAL Collab.: G. Abbiendi *et al.*, Eur. Phys. J. **C29**, 463 (2003);  
SLD Collab.: K. Abe *et al.*, Phys. Rev. **D65**, 092006 (2002);  
Erratum *ibid.*, **D66**, 079905 (2002).
201. L3 Collab.: B. Adeva *et al.*, Phys. Lett. **B261**, 177 (1991).
202. CDF Collab.: F. Abe *et al.*, Phys. Rev. Lett. **71**, 500 (1993);  
CDF Collab.: F. Abe *et al.*, Phys. Rev. Lett. **71**, 2396 (1993);  
CDF Collab.: F. Abe *et al.*, Phys. Rev. **D50**, 4252 (1994);  
CDF Collab.: F. Abe *et al.*, Phys. Rev. Lett. **75**, 1451 (1995);  
CDF Collab.: D. Acosta *et al.*, Phys. Rev. **D66**, 032002 (2002);  
CDF Collab.: D. Acosta *et al.*, Phys. Rev. **D65**, 052005 (2002);  
D0 Collab.: S. Abachi *et al.*, Phys. Rev. Lett. **74**, 3548 (1995);  
UA1 Collab.: C. Albajar *et al.*, Phys. Lett. **B186**, 237 (1987);  
UA1 Collab.: C. Albajar *et al.*, Phys. Lett. **B256**, 121 (1991);  
Erratum *ibid.*, **B272**, 497 (1991).
203. M. Cacciari and P. Nason, Phys. Rev. Lett. **89**, 122003 (2002).
204. B.A. Kniehl *et al.*, Phys. Rev. **D77**, 014011 (2008).
205. CDF Collab.: D. Acosta *et al.*, Phys. Rev. Lett. **91**, 241804 (2003);  
CDF Collab.: D. Acosta *et al.*, Phys. Rev. **D71**, 032001 (2005).
206. M. Cacciari and P. Nason, JHEP **0309**, 006 (2003);  
M. Cacciari *et al.*, JHEP **0407**, 033 (2004);  
B.A. Kniehl *et al.*, Phys. Rev. Lett. **96**, 012001 (2006).
207. ZEUS Collab.: S. Chekanov *et al.*, Phys. Rev. **D78**, 072001 (2008).
208. ZEUS Collab.: S. Chekanov *et al.*, JHEP **0902**, 032 (2009).
209. H1 Collab.: A. Aktas *et al.*, Eur. Phys. J. **C47**, 597 (2006).

## 26 17. Fragmentation functions in $e^+e^-$ , $ep$ and $pp$ collisions

210. A.H. Mueller and P. Nason, Nucl. Phys. **B266**, 265 (1986);  
M.L. Mangano and P. Nason, Phys. Lett. **B285**, 160 (1992).
211. M.H. Seymour, Nucl. Phys. **B436**, 163 (1995).
212. D.J. Miller and M.H. Seymour, Phys. Lett. **B435**, 213 (1998).
213. ALEPH Collab.: R. Barate *et al.*, Phys. Lett. **B434**, 437 (1998).
214. DELPHI Collab.: P. Abreu *et al.*, Phys. Lett. **B405**, 202 (1997).
215. L3 Collab.: M. Acciarri *et al.*, Phys. Lett. **B476**, 243 (2000).
216. OPAL Collab.: G. Abbiendi *et al.*, Eur. Phys. J. **C13**, 1 (2000).
217. SLD Collab.: K. Abe *et al.*, SLAC-PUB-8157, [hep-ex/9908028](#).